IEICE TRANS. FUNDAMENTALS, VOL.E88–A, NO.8 AUGUST 2005

PAPER Special Section on Papers Selected from the 19th Symposium on Signal Processing

A New Color Demosaicing Method Using Asymmetric Average Interpolation and Its Iteration

Yoshihisa TAKAHASHI[†a)], ***Nonmember***, **Hisakazu KIKUCHI**[†], **Shogo MURAMATSU**[†], **Yoshito ABE**[††], ***and*** **Naoki MIZUTANI**[†††], ***Members***

SUMMARY This paper presents a color demosaicing method by introducing iterative asymmetric average interpolation. Missing primary colors on a Bayer pattern color filter array (CFA) are estimated by an asymmetric average interpolation where less intensity variation is assumed to be of stronger significance, before sharpness of an initial estimate is further improved by an iterative procedure. The iteration is implemented by an observation process followed by a restoration process. The former is modeled by blurring followed by CFA sampling and the latter is completely as same as the color demosaicing method initially applied. Experimental results have shown a favorable performance in terms of PSNR and visual appearance, in particular, in sharpness recovery.

key words: *color demosaicing, interpolation, iteration, asymmetric average*

1. Introduction

Most of digital cameras use single-chip CCD sensors where a color filter array (CFA) is widely used to sample primary colors onto a Bayer pattern [1] shown in Fig. 1. As a result, a color mosaic image is acquired. Imaging process for a color mosaic image consists of a sequence of signal processing as illustrated in Fig. 2. A target scene or image passes through an anti-aliasing optical filter before sampling and quantization. On a Bayer pattern mosaic image, green samples are populated twice as many as red and blue samples, and two thirds of dense original samples are missing. The task of color demosaicing is thus to restore these missing color samples for producing a high resolution color picture which is unknown.

Owing to fewer color samples and anti-aliasing filtering, color demosaicing suffers from several difficulties. They are false color, zipper effect, blurring, quantization noise, and others. False color is a phenomenon in color reproduction where such a color different from the original is produced at a pixel of interest. False color is often generated at sharp edges and high-contrast areas, and is very noticeable over constant hue areas such as achromatic surfaces and

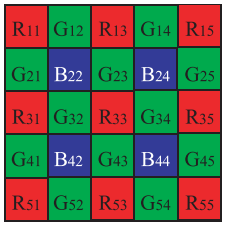

Fig. 1 Bayer pattern.

on fine texture regions. Zipper effect is a phenomenon such that originally non-existent high frequency patterns come to appear, and usually its pattern looks like a dotted line or a fringe. Zipper artifacts tend to occur along high-contrast edges and it can appear as an isolated dot at corners. False color and zipper effect can happen simultaneously, if phase-shifted interpolation would take place between different primary colors [2]. In addition, the same effect can cause different artifacts depending on the local nature of images. Such a representative phenomenon is confetti error [2] observed at bright pixels in a dark neighborhood. Blurring effect is caused by two mechanisms. The first is due to band-limiting filtering by an optical system, and the other is due to the core processing for interpolating missing samples. Quantization noise is caused by poor quantization accuracy due to spatial aperture of a CFA and aperture time in imaging, and can be sometimes objectionable at dark and highlight uniform areas.

Since there are so many problems to be solved in color demosaicing, many sorts of demosaicing algorithms are available at present [3]–[6]. Among them, Cok's constant hue-based interpolation (CHBI) is one of the greatest contributions in this topic. The hue of the color on an object surface is maintained to avoid abrupt changes in CHBI. In particular, interpolation formulae are constructed so as to keep ratios of R to G and B to G constant. Adaptive color plane interpolation (ACPI) proposed by Hamilton and Adams is one of the best-performing demosaicing algorithms ever before. In ACPI, interpolation orientation is selected so that missing samples are interpolated along edges rather than across edges. This is a spatially-adaptive interpolation, and offers favorable color reproduction quality in terms of several aspects such as false color, zipper effect, and mean squared error (MSE). Unfortunately, most of existing demosaicing algorithms produce excessively blurred images in the sense of visual perception.

Manuscript received December 10, 2004.
Manuscript revised March 10, 2005.
Final manuscript received April 28, 2005.

[†]The authors are with the Department of Electrical and Electronic Engineering, Niigata University, Niigata-shi, 950-2181 Japan.
[††]The author is with Industrial Research Institute of Niigata Prefecture, Niigata-shi, 950-0915 Japan.
[†††]The author is with Kodak Digital Product Center, Japan Ltd., Chino-shi, 391-0293 Japan.
a) E-mail: yoshi-ta@telecom0.eng.niigata-u.ac.jp

DOI: 10.1093/ietfec/e88–a.8.2108

Copyright © 2005 The Institute of Electronics, Information and Communication Engineers

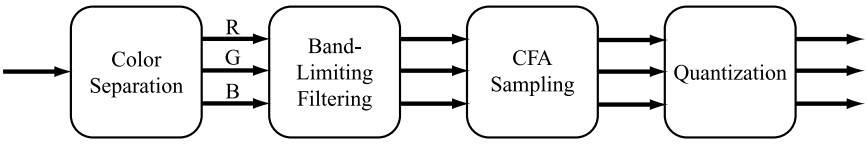

Fig. 2 Block diagram of image processing for color mosaicing.

On the other hand, digital cameras' resolution is getting higher in recent years, and there is still a strong demand for high resolution and perceptually sharp imaging. Kimmel's two-step superresolution algorithm [7] is one of the leading works along this direction. In this paper, a different approach is tried to address the problem for improving sharpness and for reducing fine artifacts for a purpose of stable visual appearance and detail restoration in demosaiced images. For detail restoration we restrict ourselves to apply short-kernel filters and introduce iterative refinements for sharpness restoration [8]. Section 2 describes a set of basic orientation/direction-adaptive interpolation for missing pixels. Section 3 describes an iterative refinement algorithm modeled by a proposed asymmetric interpolation and blurring followed by CFA sampling. Experimental results are presented in Sect. 4, and conclusions follow.

2. Interpolation of Missing Primary Colors

Missing primary colors on a Bayer pattern CCD sensor have to be interpolated to restore an unknown original picture. Among all, one of the most important guidelines is a well-known fact that neighboring primary colors are closely correlated with each other. This generally observed knowledge on natural scene pictures was sophisticated into a constant-hue principle [3] over an object surface, and any existing color demosaicing method enjoys its benefit. Since green samples are populated twice as many as those of red and blue on a Bayer pattern, missing green pixels are at first interpolated, before red and blue missing pixels are interpolated with a help of dense green pixels. Another important guideline for a better interpolation is to make an interpolation along edges rather than across them. This principle is implemented in ACPI [6] in conjunction with second-order differences, and the interpolation is spatially-adaptive and is switched among a few directional interpolations depending on the local orientation of an edge.

On the other hand, the intensity variation along an edge is not always uniform along one direction and its opposite with respect to a target pixel to be interpolated. Although, as far as the authors know, all of filtering-based interpolation schemes use symmetric averaging along edges, it can be a violation against the nonuniform intensity variations. Spatially asymmetric averaging along an edge is hence introduced in this study, where less intensity variation is assumed to be of stronger significance in a sense of stable restoration for details.

2.1 Interpolation of Missing Green Pixels

A missing green pixel on a Bayer pattern is located at a crossing point centered between two pairs of adjacent green samples at north and south and east and west orientations. In order to find the orientation of an edge, a set of parameters are defined as follows. The north-south indicator is defined by

$$\alpha = |G_{23} - G_{43}| + \gamma_n + \gamma_s \tag{1}$$

where

$$\gamma_n = |R_{13} - R_{33}| \tag{2}$$

and

$$\gamma_s = |R_{33} - R_{53}|. \tag{3}$$

In the same way, the east-west indicator is defined by

$$\beta = |G_{32} - G_{34}| + \gamma_w + \gamma_e \tag{4}$$

where

$$\gamma_w = |R_{31} - R_{33}| \tag{5}$$

and

$$\gamma_e = |R_{33} - R_{35}|. \tag{6}$$

It is a contrast that second-order differences, hence, symmetric orientation-indicators are defined in ACPI, while separate orientation-indicators are used in this work to allow independent evaluations of two opposite directions along an edge.

If $\alpha < \beta$, it indicates that a vertical change is smaller than a horizontal change, and thus it is more probable for an edge to run vertically. Contrary, if $\alpha > \beta$, an edge is assumed to run horizontally.

The next conditioning for precise inspection of variations along edges is to check a possible bias in symmetry between two opposite directions around a target pixel to be interpolated. For instance, assume that $\alpha < \beta$, and hence the edge across a target pixel lies along the north-south orientation, and if $\gamma_n < \gamma_s$, then the target green pixel value will be assumed to be closer to its north pixel value than its south. This is because strong zipper-effects are very noticeable and annoying to the human eye, and such short-distance artifacts are objectionable against sharp and stable edging lines. Hence, less variation between a pair of opposite directions along an edge is significant to reduce those artifacts

for continuous silhouette and stable sharpness around edges. As a result, a missing green pixel is estimated as follows.

If $\alpha < \beta$,

$$G_{33} = \begin{cases} \lambda_1 G_{23} + (1.0 - \lambda_1) G_{43} \\ \quad + \lambda_2 \dfrac{-R_{13} + 2R_{33} - R_{53}}{4} & (\gamma_n < \gamma_s) \\ (1.0 - \lambda_1) G_{23} + \lambda_1 G_{43} \\ \quad + \lambda_2 \dfrac{-R_{13} + 2R_{33} - R_{53}}{4} & (\gamma_n > \gamma_s) \end{cases} \tag{7}$$

where λ_1 and λ_2 are weighting factors and $0 \leq \lambda_1 \leq 1$, $0 \leq \lambda_2 \leq 1$. If $\gamma_n = \gamma_s$, it means that two variations in the opposite directions are identical, and an average of two values calculated by two right-hand side equations above is given as an estimate for the target green pixel.

In the same manner, if $\alpha > \beta$

$$G_{33} = \begin{cases} \lambda_1 G_{32} + (1.0 - \lambda_1) G_{34} \\ \quad + \lambda_2 \dfrac{-R_{31} + 2R_{33} - R_{35}}{4} & (\gamma_w < \gamma_e) \\ (1.0 - \lambda_1) G_{32} + \lambda_1 G_{34} \\ \quad + \lambda_2 \dfrac{-R_{31} + 2R_{33} - R_{35}}{4} & (\gamma_w > \gamma_e). \end{cases} \tag{8}$$

In a special case of $\gamma_w = \gamma_e$, an average of evaluation values of two right-hand side equations above is given as an estimate.

If $\alpha = \beta$, all of four right-hand side entries in Eqs. (7) and (8) are averaged as an estimate for the target.

2.2 Interpolation of Missing Red and Blue Pixels

Once all of missing green pixels have been interpolated, red and blue primary colors at missing pixel locations are estimated by the aid of dense green pixels. Since the missing pixel arrangements of red and blue are identical, the interpolation for blue primaries is explained here. There are three spatial arrangements for a missing blue pixel. In the first case, a missing blue pixel, typically as specified by B_{32} in Fig. 1, is sandwiched by a pair of blue samples. In turn, in the second case, a pair of blue samples are available to the east and the west to a missing blue pixel, B_{23}. Finally, in the third case, a missing blue pixel, typically B_{33}, is located at a face-centered position of neighboring four blue samples.

Among them, as for the first two cases, a pair of the closest blue samples is available along a specific orientation, and the pair specifies its interpolation orientation among vertical and horizontal orientations. A pair of green samples are always available along the other orientation, since demosaicing of green samples have been completed in advance. The contribution from green pixels are calculated by a second-order difference. The interpolation formulae for missing blue pixels in the first and second cases are defined by

$$B_{23} = \frac{B_{22} + B_{24}}{2} + \frac{-G_{22} + 2G_{23} - G_{24}}{2} \tag{9}$$

$$B_{32} = \frac{B_{22} + B_{42}}{2} + \frac{-G_{22} + 2G_{32} - G_{42}}{2} \tag{10}$$

and they are identical to those in ACPI.

After two types of blue pixel interpolations have been completed as above, the third case-missing blue pixels are computed. In this case, the target blue pixel originally located at a face-centered position with respect to neighboring four blue pixels now accompanies two pairs of available blue pixels at its closest vertical and horizontal positions. A better interpolation orientation is selected in a similar way to that developed for missing green pixels. However, on this occasion, a pair of orientation indicators are defined by using a simple first-order difference between a pair of adjacent green pixels either of which is located at the same position to the target blue pixel. The vertical and horizontal orientation indicators for a missing blue pixels in the third case are defined by

$$\alpha = |B_{23} - B_{43}| + |G_{23} - G_{33}| + |G_{43} - G_{33}| \tag{11}$$

$$\beta = |B_{32} - B_{34}| + |G_{32} - G_{33}| + |G_{34} - G_{33}| \tag{12}$$

respectively. Depending on a comparison between α and β, the third case-missing blue pixel is computed by

$$B_{33} = \begin{cases} \dfrac{B_{23} + B_{43}}{2} + \dfrac{-G_{23} + 2G_{33} - G_{43}}{2} & (\alpha < \beta) \\ \dfrac{B_{32} + B_{34}}{2} + \dfrac{-G_{32} + 2G_{33} - G_{34}}{2} & (\alpha > \beta). \end{cases} \tag{13}$$

If $\alpha = \beta$, all entries in the right-hand side in the above equation are averaged as an interpolation value for the target blue pixel.

3. Iterative Improvements

The color demosaicing algorithm presented in the previous section consists of a set of spatially-adaptive filtering. As same as other existing and well-performing demosaicing algorithms that are based on filtering, interpolating values for missing pixels are computed by a wide-sense lowpass filtering no matter what differential components are used and whichever the averaging is symmetric or asymmetric. Hence it is unavoidable for all of them to produce a blurred restoration to some extent due to the interpolation filtering and a band-limiting filtering involved with an optical system. In order to overcome these difficulties and to restore sharp images, an iterative procedure is introduced according to some earlier lessons [9], [10].

Let A denote a bounded linear operator on a Hilbert space, and it maps a vector, x, onto another y in the same space. Needless to mention, any digital image is represented by a vector in a Hilbert space, as long as its pixel values are bounded. A series of processes illustrated in Fig. 2 for producing a mosaic image captured on a Bayer pattern CCD sensor is assumed to be modeled by A. Also, the restoration process of demosaicing and deblurring is assumed to be modeled by an adjoint operator, B, with respect to A. Note that as long as the following equality holds for any x and y,

B is referred to as an adjoint of A [11].

$$\langle Ax, y\rangle = \langle x, By\rangle, \tag{14}$$

where $\langle a, b\rangle$ stands for an inner product between a and b.

Although it is hard to design well-performing algorithm modeled by an adjoint operator to a specific mosaicing process of A, the previously developed asymmetric average interpolation can be one of approximations among infinitely-many possible adjoint operators, because it performs color demosaicing as well or better as existing well-performing demosaicing algorithms for many images. This has been experimentally investigated.

There is another assumption in developing a geometric iteration model. Quantization is involved with the mosaicing process, and it is a nonlinear operation. Quantization is assumed to be linearized in such a way that it is replaced by an identity operator accompanying a quantization noise source. In the following development, the quantization noise is neglected.

Hence an iterative procedure is formulated in the classical Landweber-type iteration [12] as follows. Let the original image to be restored be x_0, and its color mosaic image is denoted by y_0. Since y_0 is produced by a linear system consisting of a sequence of blurring and CFA sampling, the following geometric model for the mosaicing process is valid to work.

$$y_0 = Ax_0 \tag{15}$$

Since a restored image is produced by B that is identical to the asymmetric average interpolation developed in the previous section, the following restoration model is employed.

$$By_0 = BAx_0 \tag{16}$$

Adding x_0 to both sides of the above equation before a simple manipulation, one can thus obtain

$$x_0 = By_0 + (I - BA)x_0, \tag{17}$$

where I stands for the identity operator. To convert this equation into an iterative formulation by means of a series of recurrence expressions, a conventional notation such as $x_n = By_n$, where n stands for the iteration count, is assumed. As a result, one obtains

$$x_0 = By_0 + (I - BA)x_n. \tag{18}$$

This equation is finally interpreted into an update formula by replacing the left-hand side notation and the equality symbol with x_n and a substitution symbol, respectively. The result is as follows. (Refer to [11] for mathematical details on this issue.)

$$x_n \leftarrow By_0 + (I - BA)x_{n-1} \tag{19}$$

Starting from a given mosaic image, y_0, and an initial image denoted by x_0[†] in the above equation, restoration images are successively produced.

If the above iterative formula is successively substituted into itself, it is straightforward to find another expression as follows.

$$x_n = \sum_{k=0}^{n-1}(I - BA)^k By_0 + (I - BA)^n x_0 \tag{20}$$

where n starts from one, and x_0 is given as By_0, which is a demosaiced image produced by the method in the previous section.

4. Experimental Results

For ease of reference, demosaicing by the iterative asymmetric average interpolation, which refers to the entire demosaicing method presented in this paper, is abbreviated to IAAI, whereas demosaicing by iteration-free asymmetric average interpolation described in Sect. 2 is referred to as AAI.

Our experiments are separated into two parts. In the first part, several featuring pictures are tested to make visual inspection of the characteristics of the method developed in this paper. The other part consists of several comparisons between IAAI and ACPI in terms of objective measures for natural scene pictures. Performance comparisons are made between IAAI and ACPI, because a thorough comparative study on representative existing demosaicing methods is available in Ref. [2], where ACPI is concluded as one of the best performing methods among others in a comprehensive point of view. In particular, according to the literature, ACPI outperforms best for images with sharp edges.

Two weighting factors in Eqs. (7) and (8) were fixed as $\lambda_1 = 0.6$ and $\lambda_2 = 0.4$. The number of iterations in IAAI was fixed at five. In all experiments, the anti-aliasing optical filter was simulated with the following impulse response.

$$\frac{1}{16}\begin{pmatrix}1 & 2 & 1\\ 2 & 4 & 2\\ 1 & 2 & 1\end{pmatrix} \tag{21}$$

Its transfer function is expressed by $H(z_h^{-1}, z_v^{-1}) = \frac{1}{16}(1 + z_h^{-1})^2(1 + z_v^{-1})^2$, and has a double zero at the horizontal and vertical Nyquist frequency for a digital image of which samples locate on the rectangular grid.

4.1 Visual Appearance

An orientation detection view for interpolating green primary is displayed in Fig. 3, where vertical and horizontal interpolations are printed in sky-blue and dark red, respectively. One can see that orientation-adaptive interpolation correctly works depending on local orientation of edge lines.

Figure 4 shows local fine views of IAAI and ACPI for a geometric pattern shown in (a). Note that images are magnified in their display for ease of visual inspection, and every step is equivalent to a pixel pitch. Sharp edge recovery and satisfactory color reproduction are observed in IAAI.

[†]Do not confuse this notation with the former one about x_0.

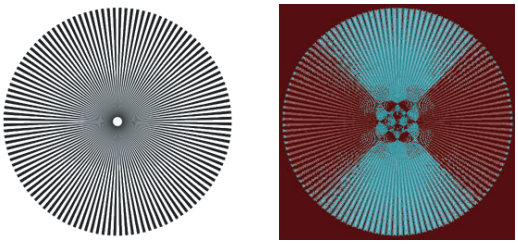

(a) (b)

Fig. 3 Orientation detection view. (a) Original picture. (b) Footprints of orientation-adaptive interpolation. Vertical in sky-blue and horizontal in dark red.

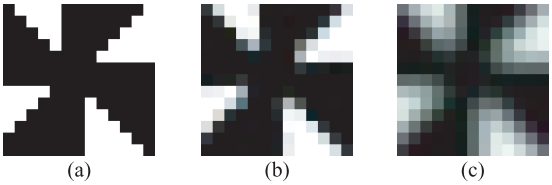

(a) (b) (c)

Fig. 4 Local fine views of interpolation. (a) Original. (b) IAAI. (c) ACPI.

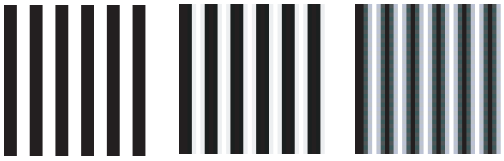

(a) (b) (c)

Fig. 5 Zipper effect inspection. (a) Original. (b) IAAI. (c) ACPI.

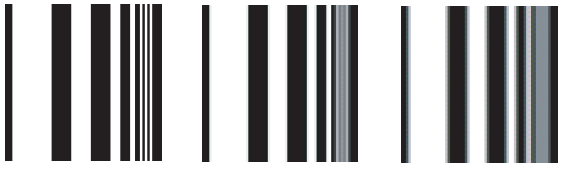

(a) (b) (c)

Fig. 6 Stripe pattern-edges inspection. (a) Original. (b) IAAI. (c) ACPI.

Figures 5 and 6 show a few demosaiced images for a visual inspection of zipper effects and false color artifacts. In particular, the original picture in Fig. 6 has a single pixel-pitch stripes that cannot be restored from a Bayer pattern mosaic image because of the worst case in the sampling theory. Objectionable zipper effects and strong false colors are noticeable to the eye in ACPI-produced images. In contrast, no zipper effects are noticeable in IAAI-produced images, and the intensity of false colors is found to be significantly weak.

Color reproduction and edge recovery for particular stripe edges/textures can be visually inspected as shown in Figs. 7 and 8. The demosaiced images by IAAI are better than those by ACPI, and sharpness recovery for edges and quite satisfactory color reproduction have been obtained.

(a) (b) (c)

Fig. 7 Color reproduction and edge recovery inspection, *left parrot*. (a) Original. (b) IAAI. (c) ACPI.

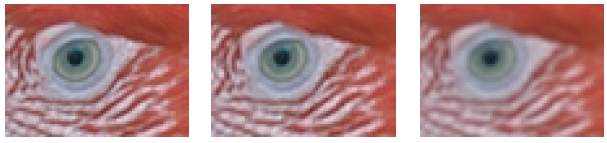

(a) (b) (c)

Fig. 8 Color reproduction and edge recovery inspection, *right parrot*. (a) Original. (b) IAAI. (c) ACPI.

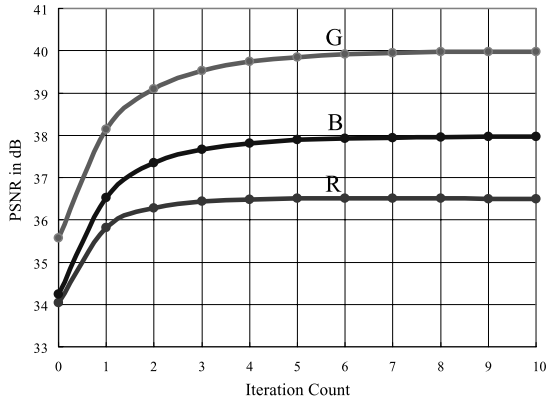

Fig. 9 Iterative PSNR improvement. Test image: *parrots* (512×768).

4.2 Objective Metrics

Figure 9 shows a plot of incremental improvements in peak-signal to noise ratio (PSNR)[†], as iteration progresses. As seen in the figure, the convergence rate of iteration is considerably fast for all primaries to reach a level close to the convergence.

Figure 10 shows a set of test images[††] used in experiments. Pixel values in original images are of 8-bit accuracy for every primary color. A part of *party* image and its color demosaicing results are shown in Fig. 11. The color reproduction by IAAI is very close to the original in visual appearance, and is sharper than that by ACPI. In particular, their difference is visually perceivable on a checker ribbon

[†]PSNR is defined by $10 \log_{10}(255^2/MSE)$, where MSE stands for mean squared error.

[††]party, picnic, portrait: Sony sRGB Standard Images, 1999. http://www.colour.org/tc8-04/test_images/Sony/
parrots: Kodak Photo CD Sampler No.3, USA IMG0060
cafeteria, bicycle: Graphic Technology -Prepress Digital Data Exchange-, Standard Colour Image Data (SCID), Japanese Standards Association, 1995.


party


picnic


portrait


parrots


bicycle


cafeteria


lighthouse

Fig. 10 Test images.


Original


AAI


IAAI


ACPI

Fig. 11 Color reproduction comparison.

and a silver fork.

Tables 1, 2, and 3 list PSNR, maximum absolute errors, and CIELAB color difference[†] ΔE^*_{ab}, respectively, for a comparison between ACPI and IAAI as well as AAI. As seen in Table 1, IAAI outperforms ACPI in every primary color reproduction. The performance of AAI which is just a core processing for IAAI is competitive to that of ACPI. A merely supplemental comment is exposed as follows; an iterative demosaicing algorithm that is made of ACPI as a substitution of AAI was experimented, and the result was discouraging.

[†]It is defined by $\Delta E^*_{ab} = \sqrt{(\Delta L^*)^2 + (\Delta a^*)^2 + (\Delta b^*)^2}$, where L^* is referred to as lightness. a^* and b^* are referred to as redness-greenness and yellowness-blueness, respectively and represent chroma components. Δ stands for the difference between two quantities in issue.

Table 1 PSNR in dB.

	Red			Green			Blue		
Image name (size)	AAI	IAAI	ACPI	AAI	IAAI	ACPI	AAI	IAAI	ACPI
party (1200×1600)	33.05	36.19	33.07	32.31	36.63	32.24	31.38	34.55	31.37
picnic (1200×1600)	34.61	35.18	34.37	34.99	35.56	34.79	33.72	33.85	33.57
portrait (1200×1600)	34.31	36.20	34.32	33.43	36.48	33.05	33.06	36.33	33.05
parrots (2048×3072)	40.40	41.40	40.38	41.51	42.75	41.36	40.40	41.26	40.42
parrots (1024×1536)	40.88	43.37	40.84	41.63	43.93	41.38	40.75	43.39	40.72
parrots (512×768)	36.43	40.20	36.46	37.10	41.57	37.03	36.18	40.90	36.19
bicycle (1920×1536)	24.69	29.42	24.62	24.54	29.21	24.48	24.03	28.50	23.96
cafeteria (1920×1536)	21.42	24.76	21.40	21.34	24.84	21.34	21.45	24.64	21.43
lighthouse (768×512)	29.37	35.02	29.35	29.57	35.08	29.57	29.74	35.13	29.70
Fig. 7(a)		30.02	23.22		29.93	23.77		29.70	22.63
Fig. 8(a)		33.33	28.25		34.36	26.96		34.30	26.14

Table 2 Maximum absolute error.

	Red			Green			Blue		
Image name (size)	AAI	IAAI	ACPI	AAI	IAAI	ACPI	AAI	IAAI	ACPI
party (1200×1600)	109	108	98	123	118	122	132	120	134
picnic (1200×1600)	130	115	136	97	84	97	121	109	121
portrait (1200×1600)	83	91	85	103	79	99	102	81	97
parrots (2048×3072)	111	56	115	54	32	53	107	62	112
parrots (1024×1536)	69	45	65	66	61	66	72	59	70
parrots (512×768)	53	40	50	46	35	43	45	27	45
bicycle (1920×1536)	174	197	169	174	197	169	180	197	173
cafeteria (1920×1536)	210	198	209	201	198	198	201	203	208
lighthouse (768×512)	106	57	92	98	60	84	98	71	92
Fig. 7(a)		45	65		61	66		59	70
Fig. 8(a)		29	42		27	43		27	45

Table 3 Color difference.

	Average			Median		
Image name (size)	AAI	IAAI	ACPI	AAI	IAAI	ACPI
party (1200×1600)	1.49	1.42	1.49	0.49	0.48	0.49
picnic (1200×1600)	3.72	3.68	3.76	0.77	0.67	0.76
portrait (1200×1600)	1.36	1.31	1.36	0.48	0.47	0.48
parrots (2048×3072)	0.48	0.41	0.49	0.39	0.37	0.39
parrots (1024×1536)	0.36	0.31	0.36	0.30	0.28	0.30
parrots (512×768)	0.51	0.40	0.51	0.37	0.31	0.37
bicycle (1920×1536)	1.96	1.63	1.96	0.91	0.82	0.91
cafeteria (1920×1536)	4.40	4.15	4.40	1.92	1.57	1.91
lighthouse (768×512)	0.92	0.61	0.92	0.51	0.44	0.51
Fig. 7(a)		1.17	2.31		0.91	1.84
Fig. 8(a)		0.81	1.56		0.67	1.25

As listed in Table 2, in most cases, the maximum absolute errors in IAAI-produced images are smaller than those in ACPI-produced images in individual color channels. On the other hand, AAI produces larger maximum absolute error than ACPI in most test images. These seemingly contradictory results imply that there are very few occasions for asymmetric interpolation to fail in faithful estimation at the expense of stable and sharp edging property. However, the excessive enhancement effect occuring at few pixels in AAI is likely modified throughout iteration.

In Table 3, CIELAB color difference, ΔE^*_{ab}, is tabulated in two statistical values of average and median. CIELAB is one of the most widely accepted device-independent color spaces. By literature [13]–[17], it is hard for the eye to perceive ΔE^*_{ab} smaller than 0.3, 0.6, 1.2, 2.3, 2.5 or 3.0. By contast, if it exceeds ten, the difference is too large for relative comparison to become insignificant [2]. The critical limit differs by literature, and of course depends on viewing conditions and the perceptual capability of individuals. It would be of benefit to give a citation to typical values of average ΔE^*_{ab} in four commercial graphic CRT monitors; 0.63, 0.83, 0.97, and 1.90 are listed in Ref. [18]. For most test images, average ΔE^*_{ab} in IAAI-produced images is around 0.4 to 1.6, excepting the cases for *picnic* (1200×1600) and *cafeteria* (1920×1536). In contrast, most of median values shows 0.3 to 0.9 which are smaller than 1.0. In addition, IAAI is found to produce smaller color difference than ACPI. It is hence reasonable to claim that color reproduction fidelity in IAAI color demosaicing is satisfactory.

5. Conclusions

In this paper, an iterative color demosaicing algorithm has been developed based on asymmetric average interpolation for Bayer pattern mosaic images. Experimental results have shown that the proposed method restores satisfactory images in most natural scene and portrait images in terms of subjective visual appearance and several objective metrics such as PSNR and CIELAB color difference.

Acknowledgement

The authors would like to thank the anonymous reviewers for their comments that helped to improve the paper.

References

[1] B.E. Bayer, "Color imaging array," U.S. Patent, no.3 971 065, 1976.
[2] R. Ramanath, W.E. Snyder, and G.L. Bilbro, "Demosaicing methods for Bayer color arrays," J. Electron. Imaging, vol.11, no.3, pp.306–315, 2002.
[3] D.R. Cok, "Signal processing method and apparatus for producing interpolated chrominance values in a sampled color image signal," U.S. Patent no.4 642 678, 1987.
[4] W.T. Freeman, "Median filter for reconstructing missing color samples," U.S. Patent no.4 724 395, 1988.
[5] C.A. Laroche and M.A. Prescott, "Apparatus and method for adaptively interpolating a full color image utilizing chrominance gradients," U.S. Patent no.5 373 322, 1994.
[6] J.F. Hamilton and J.E. Adams, "Adaptive color plane interpolation in single sensor color electronic camera," U.S. Patent no.5 629 734, 1997.
[7] R. Kimmel, "Demosaicing: Image reconstruction from color CCD samples," IEEE Trans. Image Process., vol.8, no.9, pp.1221–1228, Sept. 1999.
[8] Y. Takahashi, H. Kikuchi, S. Muramatsu, Y. Abe, and N. Mizutani, "A proposal of demosaicing and its iteration using asymmetric average interpolation," IEICE Signal Processing Symp., D3-4, pp.1–6, Yatsugatake, Nov. 2004.
[9] T. Komatsu and T. Saito, "A note on demosaicing method for single color image sensor," Inf. Technol. Lett., vol.1, pp.173–174, 2002.
[10] Y. Abe, "An iterative demosaicing algorithm," IEICE Digital Signal Processing Symp., pp.41–46, Ishigakijima, Nov. 2001.
[11] H. Stark, ed., Image Recovery: Theory and Application, Academic Press, San Diego, 1987.
[12] L. Landweber, "An iteration formula for Fredholm integral equations of the first kind," American J. Math., vol.73, pp.615–624, 1951.
[13] Y. Nayatani, Industrial Color Science, Asakura Shoten, Tokyo, 1980.
[14] J. Yamauchi and T. Kanazawa, ed., Handbook of Color Science, Nihon Shikisai-gakkai, University of Tokyo Press, Tokyo, 1980.
[15] G. Wyszecki and W.S. Stiles, Color Science: Concepts and Methods, Qualitative Data and Formulae, 2nd ed., John Wiley, New York, 1992.
[16] Y. Miyake, Analysis and Evaluation of Digital Color Images, University of Tokyo Press, Tokyo, 2000.
[17] A. Bovik, ed., Handbook of Image and Video Processing, Academic Press, San Diego, 2000.
[18] N. Katoh, K. Nakabayashi, M. Ito, and S. Ohno, "Effect of ambient light on the color appearance of softcopy images: Mixed chromatic adaptation for self-luminous displays," J. Electron. Imaging, vol.7, no.4, pp.794–806, July 1998.

Appendix: Computational Complexity

The computational complexity involved with AAI (asymmetric average interpolation) and IAAI (iterative AAI) is analyzed. It is summarized in Table A· 1 with a comparative reference to ACPI. Note that every entry shows the number of required operations per pixel, and one pixel consists of three color components of red, green, and blue. Filtering and correction imply the computation for blurring and update operation for iteration. As found in the table, AAI and ACPI have almost the same computational complexity. A single iteration in IAAI requires additional computation, which is 1.5 times high as that of AAI and ACPI. Experiments agreed with this theoretical counts. The total complexity is in proportion to the number of pixels of an image.

Table A· 1 Computational complexity per pixel.

Operations	ACPI	AAI	Filtering	Correction
additions	45.0	45.5	12.0	6.0
multiplications	19.5	16.5	18.0	0.0
absolute value	8.0	13.5	0.0	0.0
conditional branch	2.0	2.5	0.0	0.0
total	74.5	78.0	30.0	6.0

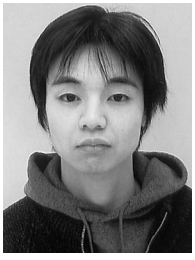

Yoshihisa Takahashi received B.E. and M.E. degrees from Niigata University in 2003 and 2005, respectively. At present, he continues his study for Ph.D. at Niigata University. His research interests include digital signal processing and image processing. He is a student member of ITE.

Hisakazu Kikuchi received B.E. and M.E. degrees from Niigata University in 1974 and 1976, respectively, and Dr.Eng. degree from Tokyo Institute of Technology in 1988. From 1976 to 1979 he worked at Information Processing Systems Laboratory, Fujitsu Ltd., Tokyo. Since 1979 he has been with Niigata University, where he is a professor of electrical engineering. He was a visiting professor at Electrical Engineering Department, University of California, Los Angeles during a year of 1992 to 1993. He holds a visiting professorship at Chongqing University of Posts and Telecommunications, China, since 2002. His research interests are in the areas of image/video processing and digital signal processing. Dr. Kikuchi is a member of IEICE, ITE, IIEEJ (Institute of Image Electronics Engineers of Japan), Japan Society for Industrial and Applied Mathematics, Research Institute of Signal Processing, IEEE, and SPIE. He served the chair of Circuits and Systems Group, IEICE, in 2000 and the general chair of Digital Signal Processing Symposium, IEICE, in 1988 and Karuizawa Workshop on Circuits and Systems, IEICE, in 1996.

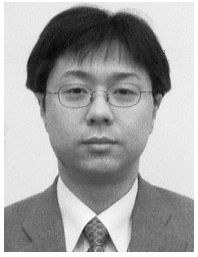

Shogo Muramatsu received B.E., M.E., and D.E. degrees in electrical engineering from Tokyo Metropolitan University in 1993, 1995, and 1998, respectively. From 1997 to 1999, he worked at Tokyo Metropolitan University. In 1999, he joined Niigata University, where he is currently an associate professor at Department of Electrical and Electronic Engineering. During a year from 2003 to 2004, he was a visiting scientist at University of Florence, Italy. His research interests are in digital signal processing, multirate systems, image processing and VLSI architecture. Dr. Muramatsu is a member of IEEE (Institute of Electrical and Electronics Engineers, Inc.), IPSJ (Information Processing Society of Japan), ITE and IIEEJ (Institute of Image Electronics Engineers of Japan).

Yoshito Abe He received the B.E., M.E., and Ph.D. degrees all in electronic engineering from Niigata University, Niigata in 1985, 1988, and 1998, respectively. In 1985, he worked at the R&D Center, Nemic-Lambda K.K., Nagaokashi. In 1988, he joined Dai Nippon Printing Co., Ltd., Tokyo, where he was a senior researcher at the Manufacturing Integration Technology Laboratory. In 2003, he leaved DNP and joined the Industrial Research Institute of Niigata Prefecture, Niigata. Dr. Abe's research interests are in digital signal processing and image processing. He is a member of the ITEJ, Imaging Society of Japan, and Research Institute of Signal Processing.

Naoki Mizutani was born in Nagano, Japan, in 1976. He received B.E., M.E., and Ph.D. degrees from Niigata University in 1999, 2001 and 2004, respectively. He works at Kodak Digital Product Center, Japan Ltd. His research interests include digital signal processing and image processing. Dr. Mizutani is a member of IEEE.